


Accurate description of the nonadiabatic proton-coupled electron-transfer process in a diabatic representation: A model study

Haifeng Song, Chaofan Li, and Changjian Xie^{*}

*Institute of Modern Physics, Northwest University, Xi'an 710127, China
and Shaanxi Key Laboratory for Theoretical Physics Frontiers, Xi'an 710127, China*

 (Received 12 September 2021; revised 6 December 2021; accepted 10 February 2022; published 23 February 2022)

Using a two-dimensional model system for the proton-coupled electron-transfer process, the eigenvalues and nonadiabatic dynamics have been notably investigated by means of diabatic representation in the Born-Oppenheimer picture. Different from a previously reported diabatic model, which was approximately determined by the eigenstates of the differently defined electronic Hamiltonians, the rigorous diabaticization was achieved by a fitting method based on the adiabatic energies and derivative couplings. As expected, the rigorous diabatic models were found to be able to accurately reproduce the eigenvalues or nonadiabatic dynamics in the adiabatic representation for three different models. Furthermore, we proposed an approximate diabatic scheme, which was built from fitting the adiabatic energies solely but with a fixed form for the off-diagonal terms in the diabatic potential energy matrix. This approximate diabatic model without the aid of the derivative coupling is shown to be as accurate as the rigorous one, which provides a simple and efficient way to accurately describe the complex proton-coupled electron-transfer processes due to accurately computing derivative couplings that are quite challenging for realistic systems.

DOI: [10.1103/PhysRevA.105.022822](https://doi.org/10.1103/PhysRevA.105.022822)

I. INTRODUCTION

Treating the coupled motion of electrons and nuclei is one of the biggest challenges in condensed-matter physics and theoretical chemistry [1–3]. Several strategic approaches, in which the electron-nuclear wave functions are represented in the full, conditional decomposition (CD) [4], exact factorization (EF) [5,6], and Born-Oppenheimer (BO) pictures [7], can be adopted in numerical calculations. In the full picture, the electrons and nuclei are treated on an equal mathematical footing, which, however, mostly becomes feasibly impossible in multiparticle systems due to the complexity of the electron-nuclear Schrödinger equation. As a result, the efficient and accurate treatments in other pictures rather than in the full picture are highly needed in practice. The separation of nuclear and electronic motions originally introduced by Born and Oppenheimer leads to the concept of the BO potential energy surface (PES) [8], which depends parametrically on the nuclear coordinates. In the EF and CD approaches, the nuclei evolve on the time-dependent PES. Alternatively, the time-independent PES is the bedrock of nuclear dynamics in the BO picture, which can be easily obtained by *ab initio* calculations for the realistic systems. Particularly, the nonadiabatic effects are brought in by including multiple adiabatic PESs and nonadiabatic couplings or a diabatic potential energy matrix (PEM) [9] in the BO picture.

A well-known model proposed by Shin and Metiu [10] provides perfect ground to develop and examine new approaches for describing the coupled motion of electrons and nuclei

efficiently and accurately. In this model system there are only three ions and an electron, in which the two end ions are fixed and the middle ion and electron are free to move in a line (see Fig. 1). The interaction terms among the three ions and an electron are simple; thus the correlated motion of the ions and electron can be rigorously described without any approximations. With the application of the Shin-Metiu model [10], many new strategies—such as an efficient multiple timescale quantum wave packet propagation algorithm [11], a quasidiabatic propagation scheme based on quasiclassical trajectories [12], an *ab initio* quantum algorithm [13], and a new surface hopping algorithm with quantum attribute [14]—for treating the electron-nuclear correlations, have been proposed to study the nonadiabatic dynamics of the proton-coupled electron-transfer (PCET) process, which plays an essential role in photosynthesis [15] and biological systems [16]. Particularly, the fundamental theoretical framework of molecular cavity quantum electrodynamics was ably designed by Taylor *et al.* [17] with the Shin-Metiu model. In addition, this model was also applied to study the property of the time-dependent expectation values of the electronic momentum operator [18] and the influence of many modes on the cavity-induced suppression of the important PCET process [19].

In the pioneering work of Shin and Metiu [10], a better understanding of the PCET process was given by the combination of the adiabatic and diabatic studies in the BO picture. They found that the fully correct description of the PCET process required three diabatic states, although the corresponding adiabatic model with two states was very accurate [10]. However, this connection between the adiabatic and diabatic representations violated the fact that the transformation between two representations is unitary [20]. In the diabaticization of Shin and Metiu, the three diabatic states incorrectly

^{*}chjxie@nwu.edu.cn

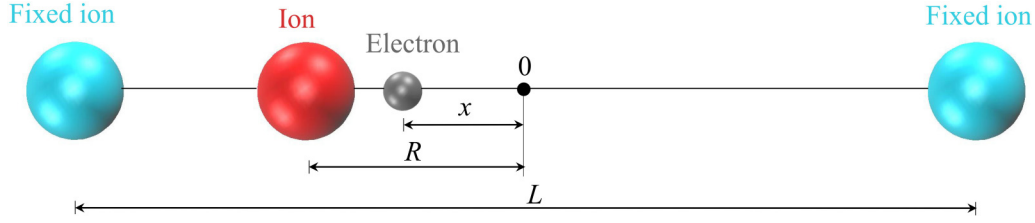


FIG. 1. Schematic representation of the Shin-Metiu model [10]. Two ions (in light blue) are fixed at the distance L . One ion (in red) and one electron (in black) can move in one dimension.

correspond to two states in adiabatic representation, which was ascribed to diabatic states approximately determined by the eigenstates of the differently defined electronic Hamiltonians. Later, several studies by means of the diabatic potentials were reported [12,17,19]. However, few studies have focused on comparison of the approaches in adiabatic and diabatic representations for this PCET model. The combination of the adiabatic and diabatic studies not only mutually verifies the accuracy of the algorithms in each representation, but also enables revealing the intrinsic mechanism of the nonadiabatic processes, such as the geometric phase effect in molecular reactions [21–23].

While the adiabatic and diabatic representations are formally identical, the usage of the diabatic representation is preferable in practice. This is because each element of the diabatic PEM is smooth [20] and the numerical convergence in the diabatic representation is much easier to achieve compared to the adiabatic representation as a conical intersection is encountered [9]. In addition, the numerical treatment in diabatic representation is much simpler in terms of the Hamiltonian as discussed below, which renders the implementation of the diabatic calculations easier and more efficient.

In this work, we aim at constructing a rigorous diabatic representation using the Shin-Metiu model [10] for the PCET process based on derivative coupling [24], in which the adiabatic and diabatic states are connected by a unitary transformation [20]. Following the work of Zhu and Yarkony [25,26], the diabaticization in this work is achieved by a fitting scheme, in which the adiabatic energies and derivative couplings are the target functions of the nuclear coordinates. The accuracy of the diabatic models is further validated by comparing the diabatic eigenvalues and dynamical results to those of the full or adiabatic models. Numerical results show that the diabatic models built by the fitting scheme are able to exactly reproduce the results in the adiabatic ones. To further explore a much simpler and more efficient but accurate diabaticization scheme for the PCET process, a fitting method with a fixed form of the off-diagonal term and adiabatic energies solely as target functions for the diabatic PEM is investigated. Its accuracy is examined by comparing the wave packet dynamics results to those obtained in the rigorous diabatic representation as well. The approach proposed in this work makes the simulation in diabatic representation much simpler and more efficient for the PCET process, since only adiabatic energies are needed without the additional calculations for derivative coupling.

This paper is organized as follows. In Sec. II, we introduce the details of solving the total Schrödinger equation of the movable ion and electron on an equal mathematical footing

exactly, potential energies of the electron in the BO picture, and accurate fitting schemes for the diabatic PEM, as well as the wave packet propagation method for studying the nuclear dynamics of the PCET process. Results and Discussion are presented in Sec. III. A brief summary is given in Sec. IV.

II. THEORY

We first show the details of solving the total Schrödinger equation of the ions and electron in the Shin-Metiu model [10] in the full picture, namely, treating the ions and electron on an equal mathematical footing, which is the benchmark for the approaches in adiabatic and diabatic representations in the BO picture as discussed below. In the Shin-Metiu model, there are three ions and one electron as shown in Fig. 1. The ions at both ends are fixed, and one ion and one electron are allowed to freely move along the line connecting two fixed ions. The donor-acceptor complexes formed by the movable ion and electron binding to two fixed ions are the reactant and product, respectively. The total Hamiltonian of the system can be written as (in atomic units)

$$\hat{H}_{\text{total}}(x, R) = -\frac{1}{2M} \frac{\partial^2}{\partial R^2} + \hat{H}_e(x, R) = \hat{T}_R + \hat{H}_e(x, R), \quad (1)$$

where R and x are the coordinates of the mobile ion and electron, respectively, with the origin at the center of the two fixed ions. M is the mass of the ion. The Hamiltonian of the electron is given by

$$\begin{aligned} \hat{H}_e(x, R) &= -\frac{1}{2} \frac{\partial^2}{\partial x^2} + V_N(R) + V_e(x, R) \\ &= \hat{T}_x + V_N(R) + V_e(x, R), \end{aligned} \quad (2)$$

in which V_N represents the interaction terms of the mobile ion with the two fixed ions:

$$V_N(R) = \frac{1}{|R - L/2|} + \frac{1}{|R + L/2|}, \quad (3)$$

and V_e are the interactions of the electron with the three ions [10,27]:

$$V_e(x, R) = -\frac{\text{erf}\left(\frac{|x-L/2|}{R_1}\right)}{|x-L/2|} - \frac{\text{erf}\left(\frac{|x+L/2|}{R_2}\right)}{|x+L/2|} - \frac{\text{erf}\left(\frac{|x-R|}{R_0}\right)}{|x-R|}. \quad (4)$$

In the above equations, L is the distance between the two fixed ions. $\text{erf}(\cdot)$ is the error function, which is the pseudopotential but more realistic and easier to fix compared to a Coulomb potential or a semiempirical potential [10,28]. R_1 , R_2 , and R_0 are the adjustable parameters for the interaction potentials.

The eigenvalues and eigenfunctions of the full Hamiltonian in Eq. (1) are determined by the total Schrödinger equation:

$$[\hat{H}^{\text{total}}(x, R) - E^{\text{total}}]\psi^{\text{total}}(x, R) = 0. \quad (5)$$

The wave function is expanded in a direct-product basis:

$$\psi(x, R) = \sum_{m,n} C_{mn} \chi_m(x) \chi_n(R) = \sum_{m,n} C_{mn} |m\rangle |n\rangle, \quad (6)$$

$$m, n = 1, 2, \dots,$$

where the basis function $\chi_l(z)$ is chosen as [29]

$$\chi_l(z) = \sqrt{\frac{2}{b-a}} \sin \left[\frac{l\pi(z-a)}{b-a} \right], \quad l = 1, 2, \dots, \quad (7)$$

with the orthonormality

$$\int_{z_a}^{z_b} \chi_l(z) \chi_{l'}(z) dz = \delta_{ll'}, \quad (8)$$

where z_a and z_b are the minimum and maximum of the range defined for the coordinate z , respectively. Since the details of the method for solving the Schrödinger's equation numerically can be found in earlier references [29,30], we only give a brief description here. The total Hamiltonian matrix elements of Eq. (1) represented in the basis of Eq. (7) are

$$\begin{aligned} [H]_{nm, n'm'} &= \langle nm | \hat{H} | n'm' \rangle \\ &= \langle nm | -\frac{1}{2M} \frac{\partial^2}{\partial R^2} | n'm' \rangle + \langle nm | -\frac{1}{2} \frac{\partial^2}{\partial x^2} | n'm' \rangle \\ &\quad + \langle nm | [V_N(R) + V_e(x, R)] | n'm' \rangle \\ &= -\frac{1}{2M} [T_1]_{nm, n'm'} - \frac{1}{2} [T_2]_{nm, n'm'} + [V]_{nm, n'm'}, \end{aligned} \quad (9)$$

where

$$[T_1]_{nm, n'm'} = -\left(\frac{n\pi}{R_b - R_a} \right)^2 \delta_{nn'} \delta_{mm'}, \quad (10a)$$

$$[T_2]_{nm, n'm'} = -\left(\frac{m\pi}{x_b - x_a} \right)^2 \delta_{nn'} \delta_{mm'}, \quad (10b)$$

where the displacement Δ is 0.0001 bohr for a given R_f . In adiabatic representation, the degree of freedom of the electronic motions is treated preferentially, which makes it much easier to solve the nuclear Schrödinger equation independently. With the same treatment of the full Hamiltonian in Eq. (9), the one-dimensional (1D) nuclear Hamiltonian matrix elements can be obtained analogously.

Another option of solving and understanding the nonadiabatic issues is to utilize the diabatic representation as discussed above. Shin and Metiu proposed a diabaticization method in which the diabatic electronic states were built upon the eigenstates of the reactant and product electronic Hamilto-

$$\begin{aligned} [V]_{nm, n'm'} &= \int_{R_a}^{R_b} \int_{x_a}^{x_b} \chi_m(x) \chi_n(R) [V_N(R) + V_e(x, R)] \\ &\quad \times \chi_{m'}(x) \chi_{n'}(R) dx dR. \end{aligned} \quad (10c)$$

The two-dimensional (2D) integrals in Eq. (10c) can be readily calculated by the 2D Gauss-Legendre quadrature. This method treats the motions of the ions and electron on an equal mathematical footing. Without any approximations, it provides the exact results for the adiabatic and diabatic models in the BO picture.

In adiabatic representation, the total wave function is expanded in terms of the adiabatic (a) electronic wave functions ($\Phi_n^{(a)}$), which depend parametrically on the ion coordinate [31]:

$$\psi^{\text{total}}(x, R) = \sum_{n=1}^{N^{\text{state}}} \Phi_n^{(a)}(x; R) \Theta_n^{(a)}(R), \quad (11)$$

in which n denotes the electronic states. Substituting Eqs. (1) and (11) into Eq. (5), the nuclear Schrödinger equation for the n th electronic state can be written as [32]

$$\begin{aligned} [\hat{T}_R + E_n^e(R) - E^{\text{total}}] \Theta_n^{(a)}(R) \\ - \sum_{n'} \left[\frac{f^{nn'}(R)}{M} \frac{\partial}{\partial R} + \frac{g^{nn'}(R)}{2M} \right] \Theta_{n'}^{(a)}(R) = 0, \end{aligned} \quad (12)$$

where $E_n^e(R)$ is the adiabatic PES and satisfies the electronic Schrödinger equation:

$$[\hat{H}_e(x, R) - E_n^e(R)] \Phi_n^{(a)}(x; R) = 0. \quad (13)$$

The nonadiabatic coupling terms

$$f^{nn'}(R) = \langle \Phi_n^{(a)}(x; R) | \frac{\partial}{\partial R} | \Phi_{n'}^{(a)}(x; R) \rangle \quad (14)$$

and

$$g^{nn'}(R) = \langle \Phi_n^{(a)}(x; R) | \frac{\partial^2}{\partial R^2} | \Phi_{n'}^{(a)}(x; R) \rangle \quad (15)$$

are the derivative coupling and diagonal Born-Oppenheimer correction (DBOC), respectively. In the calculations, the derivative coupling was calculated numerically by

$$f^{nn'}|_{R=R_f} = \frac{\langle \Phi_n^{(a)}(x; R_f) \Phi_{n'}^{(a)}(x; R_f + \Delta) \rangle - \langle \Phi_n^{(a)}(x; R_f) \Phi_{n'}^{(a)}(x; R_f - \Delta) \rangle}{2\Delta}, \quad (16)$$

nians [10]. Compared to the lowest two-state adiabatic model, it was shown that two diabatic states were not always adequate. As a result, the third diabatic state was required to reproduce the results of the two-state adiabatic model [10]. In this work, we use a rigorous diabaticization method based on the derivative coupling to construct the diabatic PESs, where the adiabatic PESs can be obtained easily by a unitary transformation. As discussed below, the newly generated two diabatic states turn out to accurately reproduce the energies of the two adiabatic states without the need of the third diabatic state.

The diabatic electronic wave functions are obtained from the adiabatic ones by the following transformation

[33]:

$$\Phi_m^{(d)}(x : R) = \sum_{n=1}^{N^{\text{state}}} U_{n,m} \Phi_n^{(a)}(x : R). \quad (17)$$

\mathbf{U} is an $N^{\text{state}} \times N^{\text{state}}$ unitary transformation matrix. Then the derivative coupling in Eq. (14) can be written as

$$\begin{aligned} f^{nm'}(R) &= \left\langle \sum_{m=1}^{N^{\text{state}}} U_{n,m} \Phi_m^{(d)}(x : R) \left| \frac{\partial}{\partial R} \right| \sum_{m'=1}^{N^{\text{state}}} U_{n',m'} \Phi_{m'}^{(d)}(x : R) \right\rangle \\ &= \sum_{m=1}^{N^{\text{state}}} U_{n,m} \frac{\partial}{\partial R} U_{n',m} + \sum_{m,m'=1}^{N^{\text{state}}} U_{n,m} \langle \Phi_m^{(d)}(x : R) | \\ &\quad \times \frac{\partial}{\partial R} | \Phi_{m'}^{(d)}(x : R) \rangle U_{n',m'}. \end{aligned} \quad (18)$$

Due to the off-diagonal derivative couplings in the diabatic representation being defined to be zero, the derivative coupling becomes

$$f^{nm'}(R) = \sum_{m=1}^{N^{\text{state}}} U_{n,m} \frac{\partial}{\partial R} U_{n',m}. \quad (19)$$

Using the application of the Hellmann-Feynman type relation gives [34,35]

$$\mathbf{f}^{nm'}(R) = \mathbf{U}_n^\dagger \frac{\partial}{\partial R} \mathbf{U}_{n'} = \frac{\mathbf{U}_n^\dagger \left(\frac{\partial}{\partial R} \mathbf{H}^d \right) \mathbf{U}_{n'}}{E_{n'}^{(a)} - E_n^{(a)}}, \quad (20)$$

where \mathbf{H}^d is the $N^{\text{state}} \times N^{\text{state}}$ diabatic potential energy matrix and $E^{(a)}$ are the corresponding adiabatic energies. The key of the diabaticization method is to determine the matrix elements H_{ij}^d of \mathbf{H}^d , namely, the diabatic PEM, for a given ion coordinate R . Following the work of Zhu and Yarkony [25,26], we use a fitting procedure to obtain H_{ij}^d , which is expanded by $\sum_k C_{ij,k} F_k$. F_k is the basis function, which can be chosen as the product of any functions with different types and orders:

$$F_k = \prod_{i=1}^m \prod_{j=1}^n p_i(R)^{\alpha_{i,j}}, \quad (21)$$

in which m is the number of the types and $\alpha_{i,j}$ is the corresponding order with the maximal number of the order n . In practice, the hyperbolic tangent function was chosen as the basis function in this work because of its high flexibility. The coefficients $C_{ij,k}$ are determined by minimizing the residual sum of squares:

$$\begin{aligned} S &= \sum_{i=1}^{N^{\text{dat}}} \sum_{n=1}^{N^{\text{state}}} (E_{n,i}^{\text{fit}} - E_{n,i}^e)^2 \\ &\quad + w \sum_{i=1}^{N^{\text{dat}}} \sum_{n=1}^{N^{\text{state}}-1} \sum_{n'=n+1}^{N^{\text{state}}} (\tilde{f}_{\text{fit},i}^{nm'} - \tilde{f}_i^{nm'})^2, \end{aligned} \quad (22)$$

where the adiabatic energies $E_{n,i}^e$ and the energy scaled derivative coupling $\tilde{f}_i^{nm'} = f_i^{nm'}(E_{n',i}^e - E_{n,i}^e)$ are computed in the

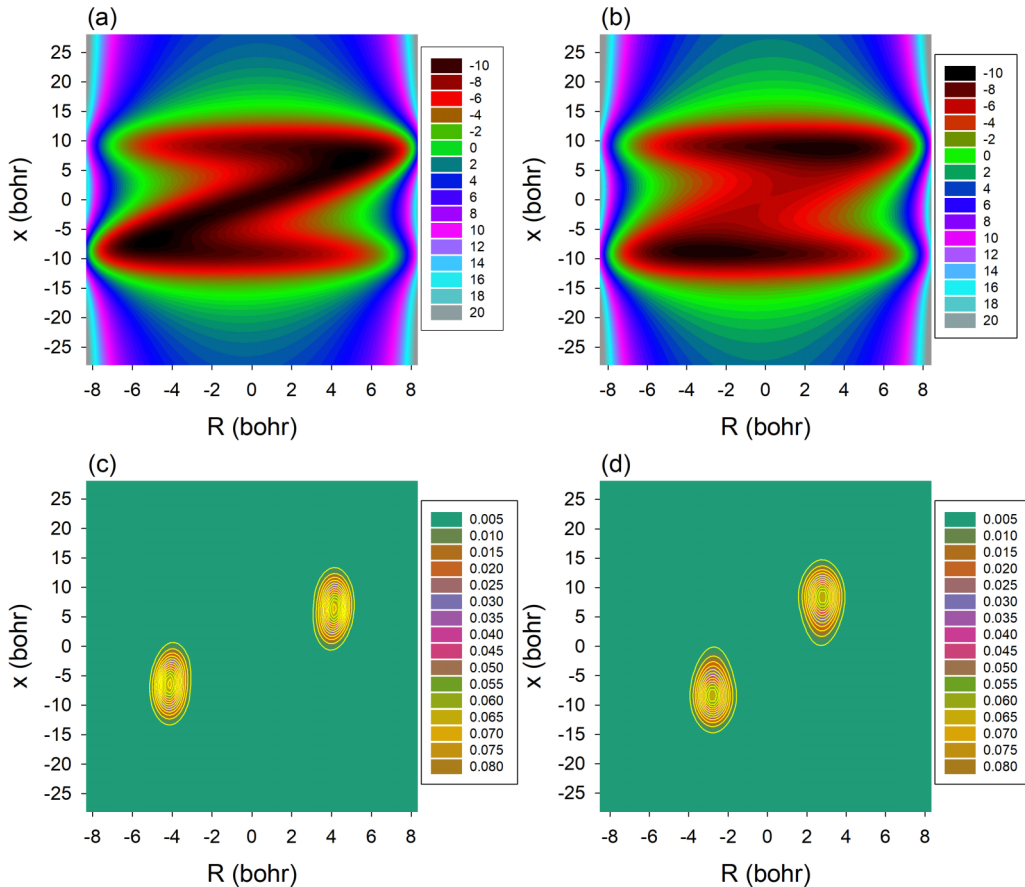


FIG. 2. Full electron-nuclear potential of models I (a) and II (b). The ions and electron wave functions of the ground state in models I (c) and II (d) in the full model.

TABLE I. Ten lowest energy levels (in eV) of model I ($R_0 = 1.50 \text{ \AA}$) and model II ($R_0 = 2.50 \text{ \AA}$).

Model I		
Exact	Two-state adiabatic	Two-state diabatic
0.00 ^a	0.00	0.00
0.072531 ^a	0.072527	0.072802
0.144050 ^a	0.144044	0.144471
0.214500 ^a	0.214489	0.214970
0.283810 ^a	0.283795	0.284256
0.351892 ^a	0.351871	0.352275
0.418638 ^a	0.418610	0.418952
0.483907 ^a	0.483872	0.484177
0.547519 ^a	0.547475	0.547782
0.609227 ^a	0.609173	0.609517
Model II		
Exact	Two-state adiabatic	Two-state diabatic
0.00 ^a	0.00	0.00
0.055348 ^a	0.055348	0.055311
0.110515 ^a	0.110515	0.110518
0.165509 ^a	0.165509	0.165474
0.220337	0.220337	0.220262
0.220339	0.220339	0.220262
0.275008	0.275008	0.275004
0.275013	0.275013	0.275009
0.329513	0.329515	0.329536
0.329551	0.329556	0.329572

^aDegenerate eigenstates.

adiabatic representation. w is a scale factor that evenly determines the relative importance of the energy and derivative coupling errors [36], which was set as 0.05 in the calculations to obtain a good fit. The Levenberg-Marquardt algorithm [37] was used to iteratively optimize the coefficients.

In diabatic representation, taking the two-state coupled system ($N^{\text{state}} = 2$), for example, the total Hamiltonian of the Shin-Metiu model can be written as

$$\hat{H}^d = \mathbf{T} + \mathbf{H}^{d,(2)} = \hat{T} \begin{pmatrix} 1 & 0 \\ 0 & 1 \end{pmatrix} + \begin{pmatrix} H_{11}^d & H_{12}^d \\ H_{21}^d & H_{22}^d \end{pmatrix}, \quad (23)$$

which is identical to the corresponding adiabatic Hamiltonian:

$$\hat{H}^a = \begin{pmatrix} \hat{T} - \frac{g^{11}(R)}{2M} & -\frac{f^{12}(R)}{M} \frac{\partial}{\partial R} \\ -\frac{f^{21}(R)}{M} \frac{\partial}{\partial R} & \hat{T} - \frac{g^{22}(R)}{2M} \end{pmatrix} + \begin{pmatrix} E_1 & 0 \\ 0 & E_2 \end{pmatrix}. \quad (24)$$

It is clear that the diabatic Hamiltonian is much simpler in form. The eigenvalues and eigenvectors of \mathbf{H}^d are the adiabatic energies (E_1 and E_2) and the unitary transformation matrix \mathbf{U} .

Once the diabatic PEM is constructed, further calculations for the energy levels or nonadiabatic dynamics are needed to examine its accuracy through comparing with the adiabatic model. As discussed below, a dynamical model of the PCET process was chosen to validate the newly constructed diabatic models. To study the nonadiabatic dynamics of the PCET process, a real wave packet method is utilized, in which the wave packet is propagated by means of the Chebyshev propagator

[38]:

$$\psi_k = 2H_s \psi_{k-1} - \psi_{k-2}, \quad k \geq 2, \quad (25)$$

with $\psi_1 = H_s \psi_0$ and $\psi_0 = \psi_i$, where ψ_i is the initial wave packet defined as the reactant. The Hamiltonian matrix is scaled to the spectral range of $(-1, 1)$ via $H_s = (H - \bar{H})/\Delta H$, in which the spectral medium $[\bar{H} = (H_{\text{max}} + H_{\text{min}})/2]$ and half width $[\Delta H = (H_{\text{max}} - H_{\text{min}})/2]$ were determined by the spectral extrema, H_{max} and H_{min} , which can be readily estimated. The time-dependent wave functions during the propagation can be readily obtained by the method of Tal-Ezer and Kosloff [39].

III. RESULTS AND DISCUSSION

Two cases of the Shin-Metiu model [10] were chosen to validate the accuracy of the diabatic models, which were built up based on the derivative coupling. The mass of the ion is 1837.15 a.u. The parameter R_0 in Eq. (4) is 1.50 \AA (denoted as model I) and 2.50 \AA (model II) with the same parameters, $L = 10 \text{ \AA}$ and $R_1 = R_2 = 1.50 \text{ \AA}$, in which the separations of two BO states are very large for two models (1.28 vs 0.05 eV). Figures 2(a) and 2(b) display the full electron-nuclear interaction potentials ($V_e + V_N$) for models I and II, respectively. In the calculations, 105 and 105 basis functions were used for the R and x coordinates of the ion and electron, respectively. One thousand and 1000 Gauss-Legendre quadrature points were used in the ranges $[-15.0, 15.0]$ and $[-4.5, 4.5]$ \AA for R and x .

The eigenstates and eigenvalues of models I and II were first computed by the exact method in the full model. Figures 2(c) and 2(d) show the wave functions of the ground eigenstate in models I and II, respectively, indicating the locally bound characteristics of the mobile electron and ion in the system. Table I lists the ten lowest energy levels of models I and II for the full (exact) and two-state adiabatic models. It clearly shows that the two-state adiabatic energies are almost identical to the exact ones (energy differences $< 0.5 \text{ cm}^{-1}$) for both models, which suggests two adiabatic electronic states are sufficiently accurate for describing the low-lying states.

For the two-state diabatic models, they were rigorously constructed from the adiabatic energies and derivative couplings. Figures 3(a) and 3(b) show the fitted results (energies and derivative couplings) of \mathbf{H}^d for models I and II compared to those from the adiabatic representation. It is clear that the fitting of \mathbf{H}^d is pretty good. The root mean square errors (RMSEs) of E_1 and E_2 are 2.80 and 2.70 cm^{-1} for model I and 1.55 and 16.57 cm^{-1} for model II. The larger RMSE of E_2 is caused by the larger energy range (0.59–8.71 eV) and more abrupt behavior of the potential energies approaching $R = 0$ in model II compared to model I. The RMSEs of the derivative coupling f are 3.30×10^{-4} and $1.86 \times 10^{-2} \text{ bohr}^{-1}$ for models I and II, respectively. The functions with different types and orders in the fitting are listed in Table II. Due to the minimal energy gap at $R = 0$ of model II (0.05 eV) being much lower than that of model I (1.28 eV), the coupling between the ion and electron in model II is much stronger than that of model I. As shown in Figs. 3(a) and 3(b), the derivative coupling in model II is much sharper than that in model I. Thus, more points were chosen near $R = 0$ in model

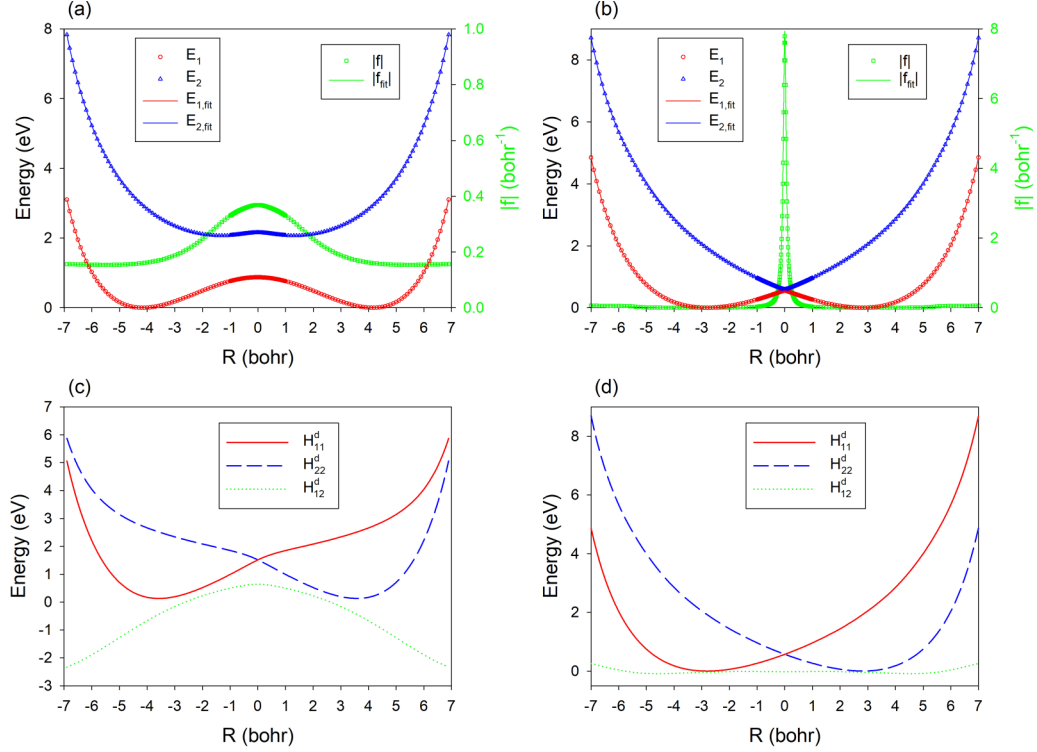


FIG. 3. The adiabatic energies E_1 (red circle) and E_2 (blue triangle) and derivative couplings f (green square) as a function of R calculated in adiabatic representation and yielded from the diabatic PEM (lines) in models I (a) and II (b). The matrix elements of \mathbf{H}^d in models I (c) and II (d).

II to fit that region better. More importantly, the symmetry of \mathbf{H}^d matrix elements in the fitting has to be considered. In

this two-state model, the diagonal elements H_{11}^d and H_{22}^d are symmetric with respect to the $R = 0$ axis, and the off-diagonal

TABLE II. Types and orders of basis functions in the fitting procedures of \mathbf{H}^d in models I and II.

Model I				
H_{11}^d	Function	Type	Order	Total order of all types
	$\tanh\left(\frac{R-C_2}{C_1}\right)$	1	$C_1 = 10.0, C_2 = -10.0$	≤ 4
		2	$C_1 = 1.0, C_2 = 0.0$	≤ 4
		3	$C_1 = 10.0, C_2 = 10.0$	≤ 4
H_{12}^d	Function	Type	Order	Total order of all types
	$\tanh\left(\frac{R-C_2}{C_1}\right)$	1	$C_1 = 10.0, C_2 = -12.5$	≤ 4
		2	$C_1 = 1.0, C_2 = 0.0$	≤ 4
		3	$C_1 = 10.0, C_2 = 12.0$	≤ 4
Model II				
H_{11}^d	Function	Type	Order	Total order of all types
	$\tanh\left(\frac{R-C_2}{C_1}\right)$	1	$C_1 = 6.0, C_2 = -7.5$	≤ 4
		2	$C_1 = 1.0, C_2 = 0.0$	≤ 4
		3	$C_1 = 1.0, C_2 = -2.0$	≤ 4
		4	$C_1 = 10.0, C_2 = 7.5$	≤ 4
H_{12}^d	Function	Type	Order	Total order of all types
	$\tanh\left(\frac{R-C_2}{C_1}\right)$	1	$C_1 = 10.0, C_2 = -1.5$	≤ 4
		2	$C_1 = 1.0, C_2 = 0.0$	≤ 4
		3	$C_1 = 8.0, C_2 = 5.5$	≤ 4

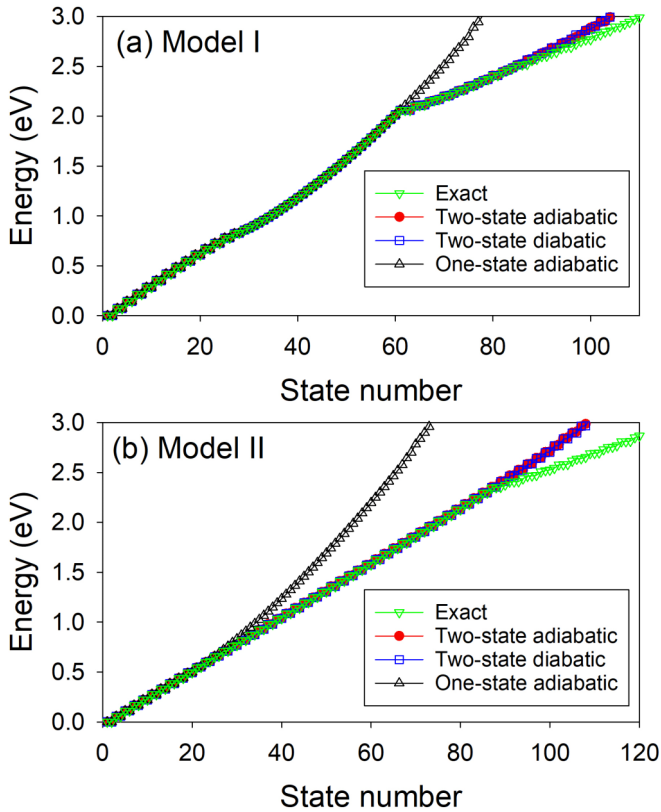


FIG. 4. Comparison of the energy levels as a function of the state number for the exact (green triangle down), two-state adiabatic (red circle), two-state diabatic (blue square), and one-state adiabatic (black triangle up) models for models I (a) and II (b).

term H_{12}^d itself is symmetric with respect to $R = 0$ as shown in Figs. 3(c) and 3(d).

As shown in Table I, the energy levels from the two-state adiabatic models were accurately reproduced by the two-state diabatic models, shedding light on the equality of the adiabatic and diabatic representations in numerics [40]. Since the potential energies in the two-state adiabatic models were calculated directly by solving Eq. (13), the small energy differences (<0.0005 eV for both models I and II) between the two-state diabatic and adiabatic models are due apparently to the fitting errors in diabatization. Compared to the three-state diabatic model corresponding to the two-state adiabatic model proposed by Shin and Metiu [10], our diabatic model with only two states is adequate for accurately describing the PCET process, in which the adiabatic and diabatic models are physically connected by a unitary transformation. Interestingly, the nonadiabatic effects have been proved to significantly influence the vibronic energy levels and to consist of the completeness for describing the nonadiabatic dynamics accurately [40]. To detect the nonadiabatic effects on the energy levels, we further calculated the energy levels up to 3.0 eV for both models, in which the excited states are energetically available. Figures 4(a) and 4(b) display the energy levels of the one-state adiabatic, two-state adiabatic, and diabatic models compared to the exact energies for models I and II, respectively. The one-state adiabatic model is derived from the standard BO approximation, where the nonadiabatic derivative coupling

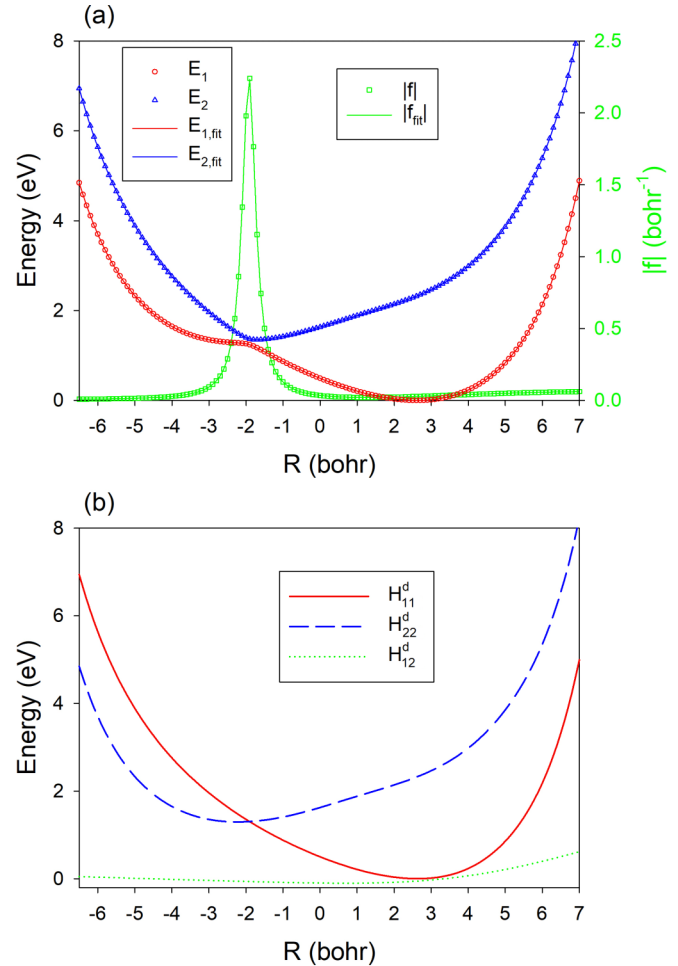


FIG. 5. The adiabatic energies E_1 (red circle) and E_2 (blue triangle) and derivative couplings f (green square) as a function of R calculated in adiabatic representation and yielded from the diabatic PEM (lines) in model III (a). The matrix elements of \mathbf{H}^d in model III (b).

and DBOC terms were neglected. It is clear that at the low-energy range, all models yield the same results. However, for higher quantum states, the one-state adiabatic model apparently overestimates the energies starting at about 2.0 and 1.0 eV for models I and II compared to two-state models, which suggests nonadiabaticity significantly influences the energetics of the systems at the high-energy range. For much higher states close to 3.0 eV, small energy differences between the two-state and exact models appear due to the contribution from higher electronic states not included in the two-state model. As expected, identical results are yielded by two-state adiabatic and diabatic models.

To further test the reliability of the diabatic model in the high-energy range and better understand the nonadiabatic dynamics of the PCET process, an asymmetric model [41] along the degree of freedom of the ion was studied in both adiabatic and diabatic representations. This model (model III) was defined by the parameters $R_0 = 5.0$ bohr, $R_1 = 3.1$ bohr, $R_2 = 4.0$ bohr, and $L = 19.0$ bohr [41]. As shown in Fig. 5, the global minimum of the ground state is located at $R =$

2.60 bohr, and two lowest electronic states are closest at $R = -1.92$ bohr with the energy gap of 0.128 eV.

The nonadiabatic dynamics of the PCET process in model III was first simulated in adiabatic representation with the two-state model following Ref. [41]. The initial wave packet is assumed to be located in the first excited state adiabatically, and the initial nuclear wave packet is a Gaussian function with the form $e^{-(R+4.0)^2/\sigma^2}$, in which the width is set as $\sigma = \sqrt{1/2.85}$ [41]. One hundred twenty-five basis functions were used in the calculations for R ranging from -6.5 to 7.0 bohrs. Figure 6(a) displays the evolution of the two adiabatic states as time varies. It is clear from the figure that the nonadiabatic transition takes place after ~ 10 fs and leads to the fluctuation of the populations of the two states with the total norm conserved during the time up to 200 fs. The time-dependent wave functions (up to 100 fs) for the ground and excited states as a function of the coordinate of the ion R are shown in Figs. 6(b) and 6(c), respectively. It is clear that the ground state grows up at $R \sim -2.0$ bohrs near the avoided crossing region, and the wave functions along the R direction for the ground and excited states are oscillatory as time increases.

For the diabatic PEM of model III obtained by the rigorous method, it reproduces the adiabatic energies and derivative couplings quite well as displayed in Fig. 5(a), and the matrix elements of \mathbf{H}^d are shown in Fig. 5(b). The RMSEs of E_1 , E_2 , and the derivative coupling f are 8.4 cm^{-1} , 9.5 cm^{-1} , and $4.52 \times 10^{-3} \text{ bohr}^{-1}$, respectively. The basis functions with different parameters and orders in the fitting are listed in Table III. Specifically, in this diabatic model the initial adiabatic wave packet needs to transform into the diabatic representation before the propagation. For a direct comparison with adiabatic representation, the unitary transformation from the diabatic to adiabatic representation was needed for the state populations and time-dependent wave functions after the propagation. As shown in Fig. 6, the results calculated from the diabatic representation are in excellent agreement with those in adiabatic representation, which validates the accuracy of the diabatic model constructed from the adiabatic energies and derivative couplings.

The derivative coupling based diabatization is the most rigorous way to determine the diabatic representation, which provides a benchmark for the approximate diabatic methods. However, the cost of computation for the derivative coupling in real systems at a high-accuracy level is very large. Thus, we further explore a diabatization scheme solely based on the adiabatic energies, which can be easily obtained from first-principles calculations in practice. For model III, we proposed a simple fitting method merely based on the adiabatic energies to construct the diabatic representation, in which the off-diagonal term H_{12}^d was imposed to have a fixed form $(R-R_c)^n$ with n equal to 0 and 1. R_c is the minimal energy gap between the two states, which is -1.92 bohr. Figure 7(a) shows the matrix elements of \mathbf{H}^d in this approximate model, and the diagonal terms are quite similar to those from the rigorously determined ones [see Fig. 5(b)]. The RMSEs of E_1 and E_2 are 18.7 and 16.8 cm^{-1} , which are slightly larger than those of

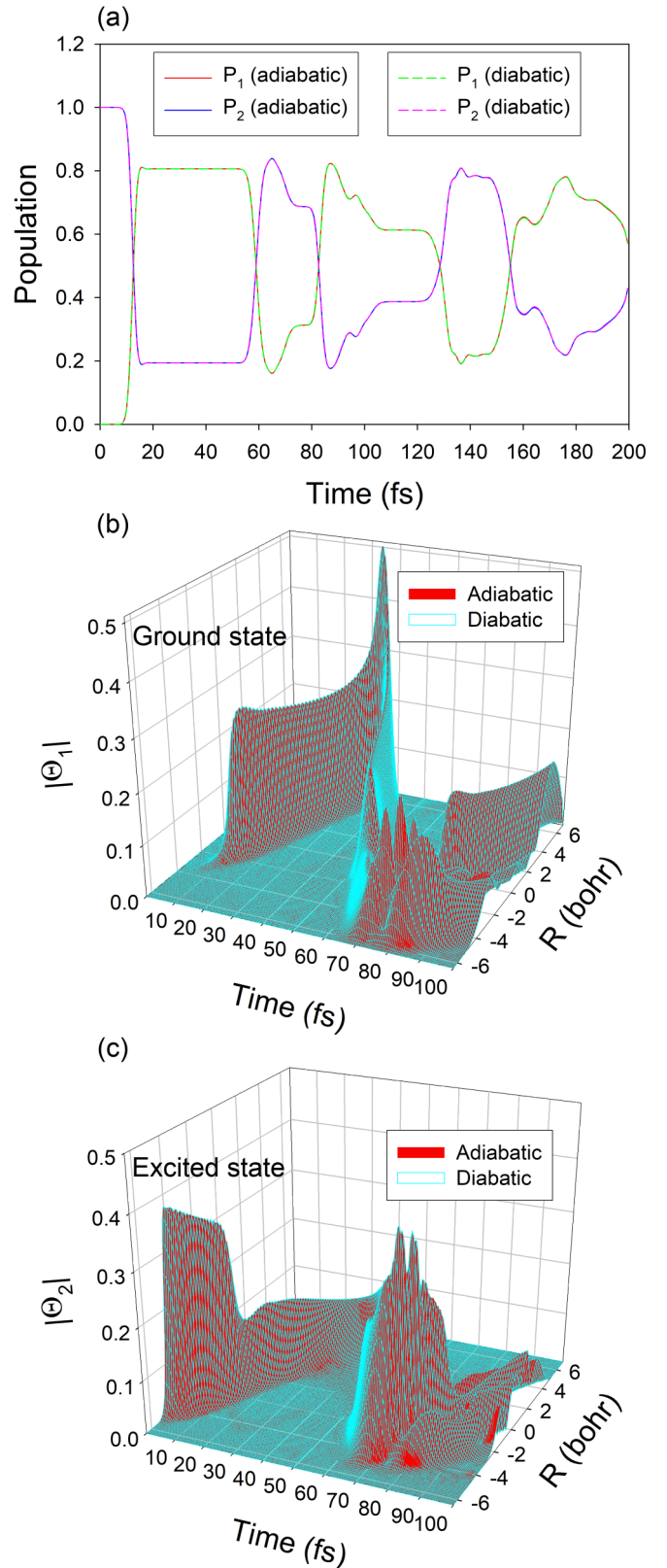


FIG. 6. Populations of the ground and excited states calculated in adiabatic (solid lines) and diabatic (dashed lines) representations as a function of time in model III (a). Time-dependent wave functions of the ground (b) and excited (c) states as a function of time and R calculated in adiabatic (in red) and diabatic (in light blue) representations.

TABLE III. Types and orders of basis functions in the fitting procedures of \mathbf{H}^d in model III.

H_{11}^d	Function	Type	Order	Total order of all types
	$\tanh\left(\frac{R-C_2}{C_1}\right)$	1	$C_1 = 6.0, C_2 = -4.0$	≤ 4
		2	$C_1 = 6.0, C_2 = 0.0$	≤ 4
		3	$C_1 = 12.0, C_2 = 4.0$	≤ 4
H_{22}^d	Function	Type	Order	Total order of all types
	$\tanh\left(\frac{R-C_2}{C_1}\right)$	1	$C_1 = 3.0, C_2 = -5.0$	≤ 4
		2	$C_1 = 6.0, C_2 = 0.2$	≤ 4
		3	$C_1 = 8.0, C_2 = 4.0$	≤ 4
H_{12}^d	Function	Type	Order	Total order of all types
	$\tanh\left(\frac{R-C_2}{C_1}\right)$	1	$C_1 = 10.0, C_2 = -2.0$	≤ 4
		2	$C_1 = 10.0, C_2 = 0.0$	≤ 4
		3	$C_1 = 10.0, C_2 = 4.0$	≤ 4

the fitting with the derivative coupling. Interestingly, it can be readily seen from Figs. 7(c) and 7(d) that the dynamical results in two diabatic models built from the fitting with and without derivative couplings are almost identical. Excellent agreement

validates the high accuracy of the fitting method merely based on the adiabatic energies with a fixed form for the off-diagonal terms $H_{ij}^d (i \neq j)$, which provides an efficient and accurate way to accurately describe complex PCET processes.

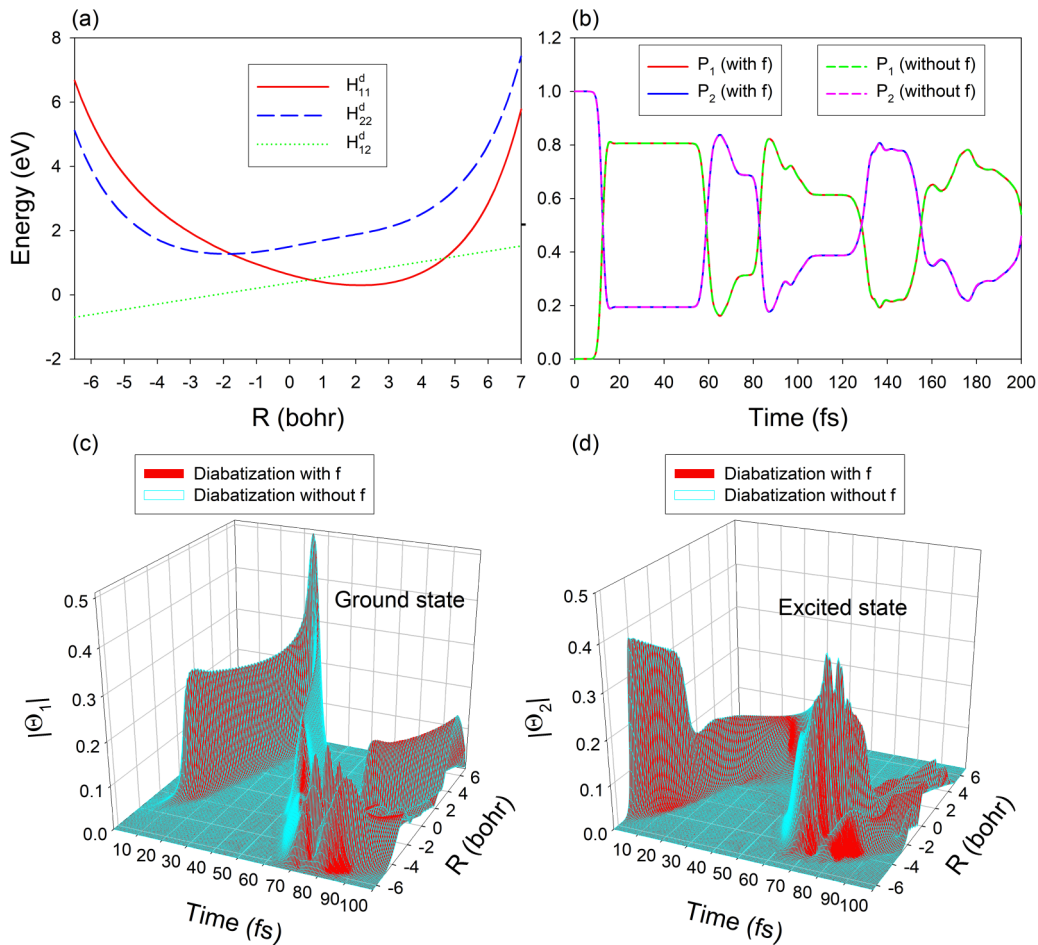


FIG. 7. The diabatic PEM in the approximation diabaticization without derivative coupling (f) for model (III) (a). Populations of the ground and excited states calculated in rigorous (solid lines) and approximate (dashed lines) diabatic models as a function of time (b). Time-dependent wave functions of the ground (c) and excited (d) states as a function of time and R calculated in rigorous (in red) and approximate (in light blue) diabatic models.

IV. CONCLUSIONS

It is usually very hard to obtain the exact solution of the total Schrödinger equation of the realistic system, in which the electrons and nuclei are treated on an equal mathematical footing due to the complexity of the full electron-nuclear Schrödinger equation. Thus, a variety of approaches based on BO PES has been proposed to treat the correlated motion of electrons and nuclei. The well-known Shin-Metiu model [10] provides a prototype to develop and examine new approaches since the coupled motion of the movable electron and ions can be completely described without any approximation. Early diabatic study of Shin and Metiu showed that a third diabatic state for the transition state is needed to accurately reproduce the results of the two-state adiabatic model [10]. This is inconsistent with common knowledge that the adiabatic and diabatic representations are connected by a unitary transformation [20]. Based on the Shin-Metiu model, we constructed a rigorous diabatic representation of the two-state models by a fitting scheme based on the adiabatic energies and derivative coupling, in which adiabatic states can be easily obtained by a unitary transformation from diabatic states. For the two chosen models, the diabatic eigenvalues were found to be almost identical to those calculated in the two-state adiabatic models. The very small energy differences (<0.0005 eV for both models I and II) between the diabatic and adiabatic models are due apparently to the fitting errors in diabatization. The identity of the adiabatic and diabatic models validates the diabatization in this work.

Furthermore, the nonadiabatic dynamics of an asymmetric PCET model [41] along the coordinate of the movable ion was investigated in both adiabatic and diabatic representations. It was found that the diabatic model exactly reproduces the results in the adiabatic model, which validates the accuracy of the diabatic model constructed from the adiabatic energies and derivative couplings. More importantly, an approximate diabatic model, which was built from fitting the adiabatic energies solely but with a fixed form for the off-diagonal terms, was shown to possess high accuracy as well. Although conical intersection is not involved for three models in this study, the diabatization scheme merely based on adiabatic potentials can be applied to the coupled PESs involving conical intersection as well [42]. It is hoped that this approximation in the fitting scheme will have the potential in the application to complex PCET processes, due to the fact that the derivative couplings in the calculations are usually expensive for the realistic systems.

ACKNOWLEDGMENTS

This work was supported by the National Natural Science Foundation of China (Grant No. 22073073). C.X. thanks the Startup Foundation of Northwest University. The Double First-Class University Construction Project of Northwest University is also acknowledged.

-
- [1] A. E. Jailaubekov, A. P. Willard, J. R. Tritsch, W.-L. Chan, N. Sai, R. Gearba, L. G. Kaake, K. J. Williams, K. Leung, P. J. Rossky, and X. Y. Zhu, *Nat. Mater.* **12**, 66 (2013).
 - [2] X. Zhou, P. Ranitovic, C. W. Hogle, J. H. D. Eland, H. C. Kapteyn, and M. M. Murnane, *Nat. Phys.* **8**, 232 (2012).
 - [3] S. K. Min, F. Agostini, and E. K. U. Gross, *Phys. Rev. Lett.* **115**, 073001 (2015).
 - [4] G. Albareda, H. Appel, I. Franco, A. Abedi, and A. Rubio, *Phys. Rev. Lett.* **113**, 083003 (2014).
 - [5] A. Abedi, N. T. Maitra, and E. K. U. Gross, *Phys. Rev. Lett.* **105**, 123002 (2010).
 - [6] B. F. E. Curchod, F. Agostini, and E. K. U. Gross, *J. Chem. Phys.* **145**, 034103 (2016).
 - [7] G. Albareda, A. Abedi, I. Tavernelli, and A. Rubio, *Phys. Rev. A* **94**, 062511 (2016).
 - [8] M. Born and J. R. Oppenheimer, *Ann. Phys.* **84**, 457 (1927).
 - [9] W. Domcke, D. R. Yarkony, and H. Köppel, *Conical Intersections: Electronic Structure, Dynamics and Spectroscopy* (World Scientific, Singapore, 2004).
 - [10] S. Shin and H. Metiu, *J. Chem. Phys.* **102**, 9285 (1995).
 - [11] S. Shin and H. Metiu, *J. Phys. Chem.* **100**, 7867 (1996).
 - [12] A. Mandal, J. S. C. Sandoval, F. A. Shakib, and P. Huo, *J. Phys. Chem. A* **123**, 2470 (2019).
 - [13] G. Albareda, A. Kelly, and A. Rubio, *Phys. Rev. Mater.* **3**, 023803 (2019).
 - [14] J.-K. Ha, I. S. Lee, and S. K. Min, *J. Phys. Chem. Lett.* **9**, 1097 (2018).
 - [15] S. J. Mora, E. Odella, G. F. Moore, D. Gust, T. A. Moore, and A. L. Moore, *Acc. Chem. Res.* **51**, 445 (2018).
 - [16] A. Migliore, N. F. Polizzi, M. J. Therien, and D. N. Beratan, *Chem. Rev.* **114**, 3381 (2014).
 - [17] M. A. D. Taylor, A. Mandal, W. Zhou, and P. Huo, *Phys. Rev. Lett.* **125**, 123602 (2020).
 - [18] T. Schaupp and V. Engel, *J. Chem. Phys.* **152**, 204310 (2020).
 - [19] N. M. Hoffmann, L. Lacombe, A. Rubio, and N. T. Maitra, *J. Chem. Phys.* **153**, 104103 (2020).
 - [20] M. Baer, *Beyond Born-Oppenheimer: Electronic Nonadiabatic Coupling Terms and Conical Intersections* (John Wiley & Sons, Hoboken, NJ, 2006).
 - [21] C. Xie, J. Ma, X. Zhu, D. R. Yarkony, D. Xie, and H. Guo, *J. Am. Chem. Soc.* **138**, 7828 (2016).
 - [22] D. Yuan, Y. Guan, W. Chen, H. Zhao, S. Yu, C. Luo, Y. Tan, T. Xie, X. Wang, Z. Sun, D. H. Zhang, and X. Yang, *Science* **362**, 1289 (2018).
 - [23] D. Yuan, Y. Huang, W. Chen, H. Zhao, S. Yu, C. Luo, Y. Tan, S. Wang, X. Wang, Z. Sun, and X. Yang, *Nat. Commun.* **11**, 3640 (2020).
 - [24] C. A. Mead, *J. Chem. Phys.* **78**, 807 (1983).
 - [25] X. Zhu and D. R. Yarkony, *J. Chem. Phys.* **136**, 174110 (2012).
 - [26] X. Zhu and D. R. Yarkony, *J. Chem. Phys.* **137**, 22A511 (2012).
 - [27] M. Sprik and M. L. Klein, *J. Chem. Phys.* **89**, 1592 (1988).
 - [28] N. P. Blake, V. Srdanov, G. D. Stucky, and H. Metiu, *J. Phys. Chem.* **99**, 2127 (1995).
 - [29] D. T. Colbert and W. H. Miller, *J. Chem. Phys.* **96**, 1982 (1992).

- [30] R. Kosloff, in *Numerical Grid Methods and Their Applications to Schrödinger's Equation*, edited by C. Cerjan (Kluwer, Dordrecht, The Netherlands, 1993), pp. 175–194.
- [31] M. Born and K. Huang, *Dynamical Theory of Crystal Lattices* (Oxford University Press, London, 1954).
- [32] C. Xie, C. L. Malbon, H. Guo, and D. R. Yarkony, *Acc. Chem. Res.* **52**, 501 (2019).
- [33] M. Baer, *Chem. Phys. Lett.* **35**, 112 (1975).
- [34] X. Zhu and D. R. Yarkony, *J. Chem. Phys.* **132**, 104101 (2010).
- [35] H. Köppel, J. Gronki, and S. Mahapatra, *J. Chem. Phys.* **115**, 2377 (2001).
- [36] A. Pukrittayakamee, M. Malshe, M. Hagan, L. M. Raff, R. Narulkar, S. Bukkapatnum, and R. Komanduri, *J. Chem. Phys.* **130**, 134101 (2009).
- [37] D. W. Marquardt, *J. Soc. Indust. Appl. Math.* **11**, 431 (1963).
- [38] H. Guo, *Rev. Comput. Chem.* **25**, 285 (2007).
- [39] H. Tal-Ezer and R. Kosloff, *J. Chem. Phys.* **81**, 3967 (1984).
- [40] C. Xie, D. R. Yarkony, and H. Guo, *Phys. Rev. A* **95**, 022104 (2017).
- [41] F. Agostini, A. Abedi, and E. K. U. Gross, *J. Chem. Phys.* **141**, 214101 (2014).
- [42] C. Li, S. Hou, and C. Xie, *Chin. J. Chem. Phys.* **34**, 825 (2021).